JSEE Vol. 26, No. 3, 2024 DOI: 10.48303/jsee.2024.2029664.1091

Research Paper

Evaluation of Steel Tall Buildings with Post-Tensioned Cables Subjected to Sequences Far from Fault

Mehran Akhavan Salmassi[1] and Mohsen Gerami[2*]

1. Ph.D. in Structural Engineering, Islamic Azad University, Semnan Branch, Semnan, Iran
2. Professor of Earthquake Engineering, Semnan University, Semnan, Iran, *Corresponding Author; email: mgerami@semnan.ac.ir

Received: 19/05/2024
Revised: 02/07/2024
Accepted: 09/07/2024

Keywords:
Post-tensioned cables; Tall buildings; Far from fault; Sequences records; Steel structures

ABSTRACT

Lateral forces, especially seismic forces, cause significant damage to structures, especially tall ones. On the other hand, sequence earthquakes also cause irreparable damage to structures. Therefore, post-tensioned connections are one way to improve structures' seismic behavior. This study investigated 12-story tall steel structures with simple flexural connections and post-tensioned connections in two dimensions and 5- and 8-story structures with simple flexural connections and post-tensioned connections in two dimensions under sequences earthquakes. In this study, the beam and column sections of the sarees mentioned above were designed with ETABS software and simulated with OpenSees software to apply sequence records. The previous simulation was validated, and the structures were analyzed non-linearly under sequence records. The results indicated that the maximum drift angle was reduced by 50% in the 12-story structure with post-tensioned connections. As a result, post-tensioned connections improved the behavior of tall structures.

How to cite the article:
Akhavan Salmassi, M., & Gerami, M. (2024). Evaluation of Steel Tall Building with Post-Tensioned Cables Subjected to Sequences Far from Fault. *Journal of Seismology and Earthquake Engineering*, *26*(3), 9-24. DOI: 10.48303/jsee.2024.2029664.1091

Copyright © 2024 IIEES. Published by International Institute of Earthquake Engineering and Seismology.
This work is licensed under a Creative Commons Attribution-NonCommercial 4.0 International license (https://creativecommons.org/licenses/by-nc/4.0/). Non-commercial uses of the work are permitted, provided the original work is properly cited.

1. Introduction

Unexpected ruptures were observed in the beam-to-column connections of steel flexural frames in the Northridge earthquake. Ricles et al. proposed pulled-back connections with upper and lower angles in 2001, and Christopoulos et al. proposed pulled-back connections with energy-dissipating bars in 2002 as an alternative to welded connections for steel flexural frames (Figure 1).

Unexpected ruptures were observed in the beam-to-column connections of steel flexural frames in the Northridge earthquake. By Ricles et al. in 2001, pulled-back connections with upper and lower angles and by Christopoulos et al. in 2002, pulled-back connections with energy-dissipating bars were proposed as an alternative to welded connections for steel flexural frames (Christopoulos et al., 2002).

On the other hand, according to the World Green Building Council's challenge, all buildings must be designed to achieve net zero operating carbon by 2030 and net-zero embodied carbon by 2050. Twenty years ago, the Jin Mao Tower was built distinctively for several objectives, and those goals have been advanced thanks to ideas. Not only did it become China's tallest building at the time, it also transformed the country's wind and seismic engineering codes and, most significantly, paved the way for subsequent buildings to adopt resilient design principles. The principles of life-cycle engineering and eco-conscious design informed the development of these systems. The Jin Mao Tower inspired several innovative and economic tall building structural systems, including core-connected mega-columns, friction-fused seismic systems, optimization theory applications, and carbon concerns during construction. Issues from research into building work that integrates these concepts with future opportunity views are the topic of this article. Plans that consider machine learning and self-sufficiency will be considered as we review carbon calculation techniques (Sarkisian, 2022). In addition, several regions across the globe have recorded seismic sequences, defined as a series of medium-strong earthquake ground motions that happen very quickly after each other. The consequences of these occurrences on steel buildings are examined in the article. Seismic sequences have been used to study rigid-plastic systems with one degree of freedom (SDOF), moment-resistant frames with stiff and semi-rigid joints, and a concentrically braced steel frame. There is a noticeable buildup of damage in the case of just one occurrence for both the SDOF systems and the steel frames. A strategy is put forward to reduce the q-factor based on the idea that, to verify damage control limit states, the seismic analysis of a non-linear system is conducted using an elastic analysis with the q-factor. This behavior-based decrease should be considered in areas prone to earthquakes, where the likelihood of repeated seismic events is significant (Fragiacomo et al., 2004).

As shown in this paper, some others zeroed in on the ductility requirement spectra for SDOF systems, which are subjected to many near- and far-fault seismic ground motions. The most novel aspect is the first attempt to quantify the seismic

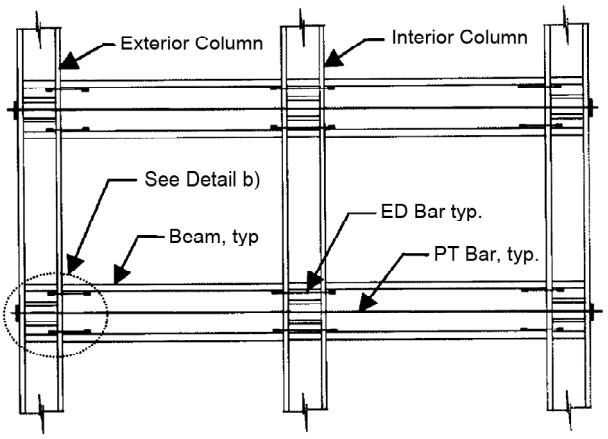

(a) Steel Frame with Energy-Dissipating Post-Tensioned Connections

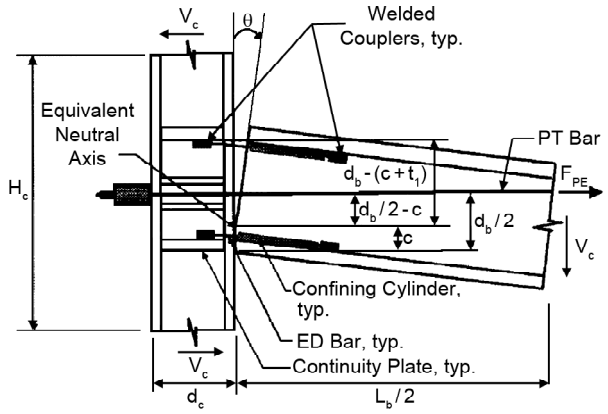

(b) Free-Body Diagram of an External Post-Tensioned Connection

Figure 1. Details of the proposal by Christopoulos et al. in 2002.

sequence effect regarding ductility needs properly; this phenomenon has previously received little attention. Artificial sequences, formed by a rational and random combination of real single events, are the only ones examined in this work due to the absence of records of real seismic sequences. An analysis of over 120 million dynamic inelastic analyses is carried out statistically to derive expressions for the ductility requirements regarding vibration period, viscous damping, post-yield stiffness, and force reduction factor. The seismic sequence effect proves that considering just the 'design earthquake' is inadequate; according to this conventional wisdom, doing so results in underestimating structural damage as ductility demands are underestimated (Hatzigeorgiou, 2010). The other study found that the sub-assemblies could tolerate an inter storey drift of 4% without strength loss, provided they were connected using post-tensioned steel connections made with strands and decreased flange plates (Chou et al., 2006). An analysis of beam-to-column connections in precast concrete revealed that the study's ultimate goal was to design a cheap and straightforward moment-resistant precast concrete connection (Cheok & Lew, 1991). The idea of using beam prestressing tendons debonded at the junction and extending a certain distance on either side of the column to connect precast concrete frame elements is presented. The results demonstrate that this configuration will improve joint shear performance and restore force characteristics. Structures with lengthy natural periods should have a peak displacement reaction comparable to conventionally prestressed concrete systems, according to dynamic inelastic calculations; systems with elastoplastic hysteretic properties should have a somewhat bigger peak displacement response.

To illustrate how to compute the force-deformation properties of precast concrete frame systems using this notion, an appendix contains a numerical design example (Priestley & Tao, 1993). Others looked into post-tensioned precast concrete walls without any boundaries. The results showed that after an earthquake, unbounded post-tensioned precast walls drifted more than cast-in-place walls but accumulated much less residual drift (Kurama et al., 1999). An analysis of post-tensioning in steel structures revealed that, when subjected to the earthquake records under study, the seismic performance of a post-tensioned steel MRF outperformed the performance of an MRF with normal welded connections (Ricles et al., 2001). An experimental assessment of post-tensioned steel connections' ability to withstand earthquakes is presented.

To predict the connection decompression moment and moment capacity and the increase in post-tensioning strand force owing to connection deformation, simple design models are constructed and verified by the test results (Ricles et al., 2002). To achieve ductile behavior under earthquake excitations, new moment-resisting connections were advised to be constructed with distinct details after the 1994 Northridge earthquake. The primary goal of these details was to prevent weld failure and direct inelastic beam deformation into the beam's interior span instead of the joint connection area. Researchers suggested using post-tensioned moment connections in moment-resisting frames as an alternative to welded moment-resisting connections for earthquake loading resistance. The seismic response of the links is the focus of this research. High-strength steel cables, which make up post-tensioned connections, are set up parallel to the webs of the beams, passed through the column, and finally fastened at the face of the column's flange. Steel cables have multiple purposes: first, they compress the beam and column flanges; second, they provide the resisting moment of connections against applied service loads; and third, they eventually cause the columns to self-center, meaning that they will return to their original position after being tilted by an earthquake. To further reduce the seismic stress felt at the joints, two steel angle sections are fastened to the upper and lower surfaces of the connections.

Past studies have shown that post-tensioned connections in moment-resistant steel frames lessen seismic (Gerami & Khatami, 2017). The Northridge earthquake of 1994 caused the collapse of numerous welded steel moment-resisting frames (WSMRF) in the beam-to-column connection area. Damage to WSMRF altered its attitude,

going against what the engineers had anticipated. As a result, engineers opted to incorporate more intricate and ductile connections. Post-tensioned connection (PTC) stands out of the novel connections they suggest. PTC uses energy dissipation to manage plastic deformation and high-strength, pre-tensioned wires to produce self-centering characteristics. The PTC was numerically modeled in this study using the ABAQUS finite element program. In addition to comparing the model's accuracy to experimental results, this study models six different types of connections and investigates how different parameters, such as the ratio of length to thickness, the use of high-strength steel (HSS) angles, the application of angles with unequal leg lengths, and the use of angle stiffness, affect the connections' behavior under cyclic loading. This paper's models demonstrate that using HSS at an angle increases flexural strength and lateral load-bearing capacity by a small amount. Additionally, the results showed that the connection's behavior is unaffected by using an angle with unequal leg length. Enhancements to bending strength, capacity, energy dissipation, initial and inelastic stiffness, and durability can be achieved by using stiffness for angle. Additionally, the energy dissipation in the connection would be 17% higher with a lower g/t ratio, as the gauge length-to-thickness ratio would be reduced from 4 to 3.6 (Azizi & Siahpolo, 2019). Two welded stiffened plates on each of the beam flanges are recommended to constrain the tendons at the mid-span of the beams, as recommended by seismic rehabilitation of bolted end plate connections with post-tensioned tendons (Saberi et al., 2016). The performance of steel moment frames was found to decrease by 37.6% when post-tensioned connections were only implemented on two of the six floors (Tafreshi & Gerami, 2021) and by 29.4% when post-tensioned connections were only implemented on the last three floors. The performance of the MRF with optimal PTED connections exceeds that of the MRFs with conventional moment-resisting connections for a specified seismic environment, according to other research about the Computational Framework for Automated Seismic Design of Steel Frames with Self-Centering Connections (Apostolakis et al., 2014). Furthermore, Shen and Akbas (1999) found in their study of the Seismic Energy Demand in Steel Moment Frames that the energy concept based on the single degree of freedom has limits when extended to the practical structural system for design purposes. The evaluation focuses on the 6-story SC-MRF building's seismic performance and economic seismic losses caused by post-tensioned (PT) connections with top-and-seat angles. In this work, we build and validate a phenomenological model of PT connection lateral load response based on experimental data.

The newly established phenomenological model generates a 2D model of the 6-story SC-MRF in OpenSees. The WMRF with reduced beam section (RBS) connections is similarly modeled using the same member sizes as the SC-MRF. The SC-MRF and WMRF models undergo incremental dynamic and nonlinear static evaluations, respectively. The WMRF has a 40% higher lateral load-carrying capacity than the SC-MRF. The dynamic analysis results demonstrate that the WMRF exhibits more resilience to collapse than the SC-MRF, which experiences fewer residual drifts. Lastly, the FEMA P58 technique is used to evaluate the earthquake's economic impact on the two buildings. The SC-MRF is projected to suffer a 21% larger annual loss than the WMRF building. Specifically, the SC-MRF structure (with PT connections and top-and-seat angles) experiences higher collapse losses but lower projected losses due to excessive residual drifts (Guan et al., 2018). ABAQUS FEA modeling of seismic retrofitting of RC structures using precast prestressed concrete braces showed that the retrofitting system had low stiffness and was not effective in minimizing lateral drift when the compression strength of the brace was less than that of the existing frame (Nateghi Alahi & Vatandoost, 2018). The analysis method can accurately capture the various failure modes, as shown by numerical modeling of failure in steel post-tensioned connections subjected to cyclic loading (Al Kajbaf et al., 2018). The dynamic response of FDPT frames was compared with that of traditional frame structures (Zhao et al., 2020) in a study that assessed the likelihood of

progressive collapse in friction-damped post-tensioned steel frames using a simplified model. While a benchmark for designing hexagonal castellated beams in the PT semi-rigid connections has been established thanks to research into the cyclic behavior of such beams in steel moment-resisting frames with post-tensioned connections, a step-by-step design guideline is still needed before such beams can be incorporated into design codes and specifications for steel structures (Sarvestani, 2017). An increase in flexural capacity and a decrease in ductility were seen in beams strengthened by post-tensioned external reinforcing bars in an experimental study and modeling of reinforced concrete beams (Doostdar et al., 2010). Kim and Christopoulos (2008a) found that friction-damped post-tensioned self-centering connections can achieve stiffness and strength similar to welded connections in steel moment-resisting frames.

According to research on self-centering seismic lateral force resisting systems (Chancellor et al., 2014), such systems can mitigate or prevent structural damage to irreplaceable elements by dampening the structural response elastically via gap opening mechanisms.

Compared to moment frames with rigid welded connections, seismic behavior is enhanced when post-tensioned connections are used in flexible steel frame structures (Akhavan Salmassi et al., 2019). A 23% increase in failure probability has been found when optimizing the reliability of post-tensioned self-centering rocking steel frame structures without accounting for uncertainties (Lavaei et al., 2023) based on reliability-based design. Others looked for seismic behavior in post-tensioned self-centering concrete frames subjected to ground vibrations resembling pulses from a nearby fault. Guidelines and recommendations for designing PTSC frames are presented based on the results and observations of structural performance concerning pulse characteristics (Li et al., 2023). There has been a lot of research on high-strength concrete, but not nearly as much on high-strength steel reinforcing. Limiting the yield strength of transverse reinforcement is done to regulate the width of diagonal cracks and to guarantee that the reinforcement yields before brittle failure mode sets in, according to four current design codes: ACI 318-14, Eurocode 2, CSA A23.3-04, and JSCE-07. JSCE-07 sets a limit of 800 MPa for transverse reinforcement when the compressive strength of concrete exceeds 60 MPa, in contrast to ACI, Eurocode 2, and CSA A23.3-04, which all set limitations of 420, 600, and 500 MPa, respectively. It was determined in this work how to perform high-strength transverse reinforcement in prestressed concrete (PSC) and reinforced concrete (RC) beams. The code constraints were exceeded by 16 beams that were monotonically loaded to failure and reinforced with stirrups with yield strength greater than that. Before flexural failure could occur, shear failure was intended for all beams. Despite specimens reinforced with stirrups with strengths greater than 420 mph, most test findings demonstrated stirrup yielding and crack widths that were less than the code requirements. Regarding serviceability, the test findings suggest that high-strength stirrups can be used with PSC beams (Lee et al., 2020).

Using OpenSees software, an evaluation of steel flexural frames with post-tensioned cables subjected to seismic sequences far from the fault was performed. Incremental nonlinear dynamic analysis of 5, 8, and 12-story frames in two cases of flexural structures with simple rigid connections and connections with post-tensioned cables was performed.

2. Flexural behavior of Energy-Dissipating Post-Tensioned Connections

Energy-dissipating rebars and a combination of them are shown in Figure (2) under the effect of cyclic loading of the moment-of-rotation relationship (M-θ_r) at the interface of the beam and column for post-tensioned rebars. The total moment in the PTED connection is obtained from the sum of the moments created by the post-tensioned rebars (MPT) and energy dissipating bars (MED), which is equal to:

$$M_{PTED} = M_{PT} + M_{ED} \tag{1}$$

This combination of moment-rotation relationships shows a hysteresis behavior as a flag in

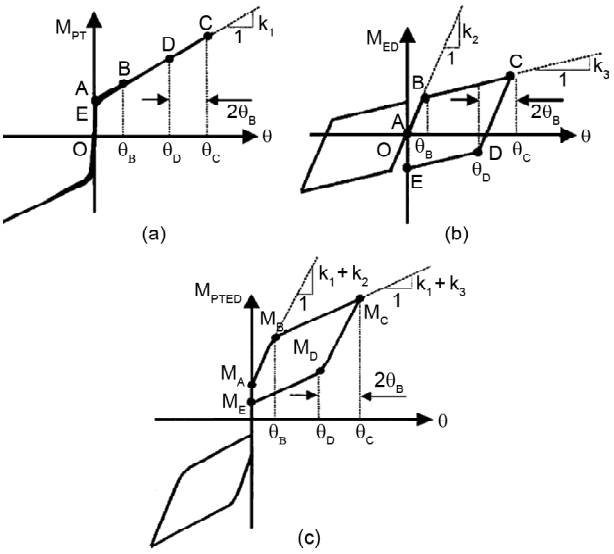

Figure 2. Idealized hysteresis behavior of energy-dissipating post-tensioned connections (a) Participation of tensioning rebars (b) Participation of energy-dissipating rebars (c) Moment-period relation of post-tensioned connections with energy-dissipating elements (Christopoulos et al., 2002).

Figure (2c). Although the system maintains its self-centering capability, it dissipates energy when a negative moment is created at the beam-column interface. As long as complete contact between the beam and the column are established, the PTED connection behaves elastically; until this stage, the post-tensioning force (PT) is sufficient to maintain complete contact between the beam and the column. Therefore, there is no opening in the seam between points O and A in Figure (2) (Christopoulos et al., 2002).

The PT force controls the value of the flexural moment MA, after which the connection between the beam and the column are opened. When the value of the flexural moment reaches MA, the seam is opened, and the rotational stiffness of the PTED connection is provided by the elastic stiffness of the two upper and lower energy-dissipating bars and post-tensioning bars (from point A to point B in Figure (2)). In this case, the behavior of the connection is non-linear elastic due to the opening of the behavior. This non-linear elastic behavior will continue until the value of the flexural moment reaches MB. This moment is related to the tensile yield capacity of ED bars and is defined by Equation (2):

$$M_B = M_A + (k_1 + k_2)\theta_B \tag{2}$$

In which k_1 is the rotational elastic stiffness of the PT rebars, k_2 is the elastic rotational stiffness of the upper energy dissipating rebars, and θ_B is the rotational stiffness in which the tensile yielding of the upper dissipating rebars begins. In the continuation of loading, the rotational stiffness of the post-tensioned connection is provided by the elastic stiffness of the post-tensioned cables and the stiffness after yielding the energy-dissipating rebars (from point B to point C in Figure (2)). At this stage, the connection behavior is non-linear elastic behavior due to the continued opening at the interface of the beam and column. This behavior takes place until the maximum rotation occurs in each cycle (θ_C). The moment value at this point is obtained from Equation 2:

$$M_C = M_B + (k_1 + k_3)(\theta_C - \theta_B) \tag{3}$$

k_3 is the rotational stiffness of energy-dissipating bars after their yielding.

The PTED connection, until reaching the compressive yield capacity of the energy-dissipating upper rebars (from point *C* to point *D* in Figure (2)), shows nonlinear elastic behavior by changing flexural direction. At this point, the connection period (θ_D) and connection moment (M_D) is calculated from the following relations:

$$\begin{aligned} &\theta_D = \theta_C - 2\theta_B \\ &M_D = M_C - (k_1 + k_2)(2\theta_B) \end{aligned} \tag{4}$$

The occurrence of non-linear elastic behavior is possible only if the buckling of the upper dissipative bars is prevented in pressure. The energy until re-establishing full contact between the beam and the column (from point *D* to point *E* in Figure (2)) of the PTED connection shows nonlinear elastic stiffness during the compressive yielding of the upper dissipative bars. The corresponding flexural moment is obtained from the following relation:

$$\begin{aligned} &M_E = M_D - (k_1 + k_3)\theta_D = \\ &M_D - (k_1 + k_3)(\theta_C - 2\theta_B) \end{aligned} \tag{5}$$

As shown in Figure (2), the behavior of the PTED connection in the positive opposite half-cycle, loading in which the tensile and compressive yielding of the energy-dissipating lower rebars is symmetrical.

3. Shear behavior of Energy-Dissipating Post-tensioned Connections

If a suitable post-tensioning force is applied, no physical shear connection between the beam and column will be required. Shear transfer can be sufficiently provided by Coulomb friction at the beam-to-column interface. Preparing the contact surfaces by sandblasting them dramatically increases the friction coefficient of the two surfaces. As long as there is no interference at the moment characteristics of the PTED connection, other methods can be used for shear transfer. These methods can include shear transfer parts with horizontal slots connected to the beam or flexible seating angles that can change shape without increasing the capacity (Christopoulos et al., 2002) (Kim & Christopoulos, 2008b).

4. Post-tensioned Connections Modeling

STEEL 02 steel material with isotropic hardening models post-tensioned connections in OpenSees software in beam-column materials (Figures (3) and (4)) (Mazzoni et al., 2007). Cable material is a type of elastic material. It is used to define elastic uniaxial material. Among the elastic materials that are selected in the materials of the dampers, with the difference that in the Uniaxial Material Elastic command, there is a parameter called damping tangent. This command indicates that zero length or the element with zero length is used in the opening of the connection due to the opening in the connection to model this area; the

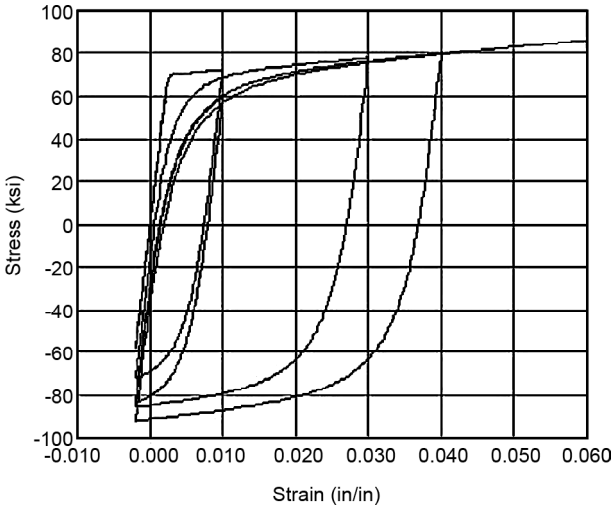

Figure 3. Hysteric behavior of Steel02 with isotropic hardening in pressure.

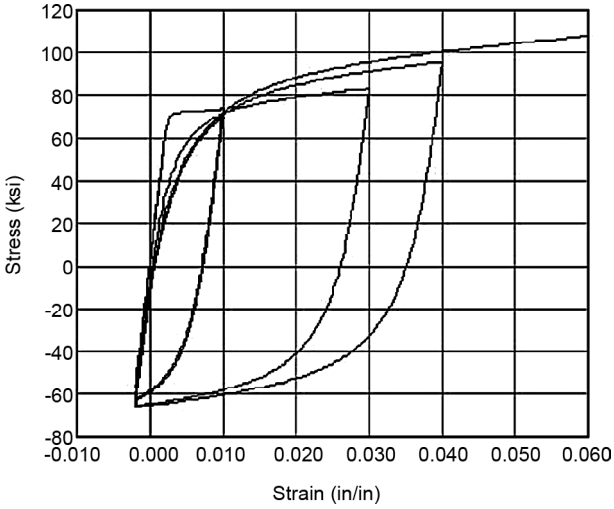

Figure 4. Hysteric behavior of Steel02 with isotropic hardening in tension.

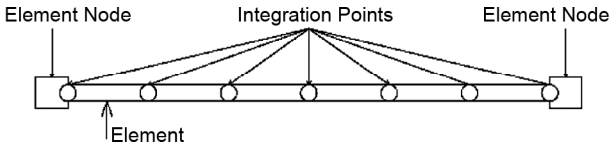

Figure 5. Number of integration points in the members.

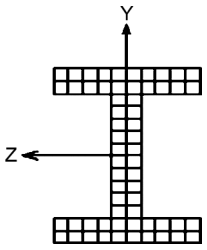

Figure 6. Fiber section of beam and column materials.

Equal DOF command also applies the dependence related to the degrees of freedom. In this command, one node is part of the reference node, and others are dependent on the reference node. Figure (5) also shows the number of member integration points, and Figure (6) indicates the fiber section of beam and column materials.

5. Verification and Validation

OPENSEES software and Rickes et al. (2001) Figure (7) checked the modeling accuracy. This article analyzes a 6-story, 6-span frame with particular flexural joints. DRAIN-2DX software is used in the design. The soil type is D, and the beam and column are 50, 36, and 572, respectively. The dead and live loads on the floors are 2.40 kpa and 4.9 kpa, respectively, and the dead and live loads on the roof are 0.964.79 pa, respectively.

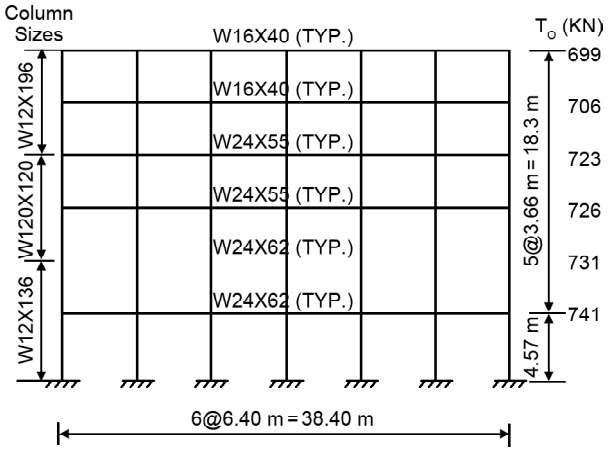

Figure 7. Flexural frame with six floors and six openings.

The investigation indicates that the building in question was verified by applying the effect of the 1940 El Centro record. For earthquake engineers, the El Centro earthquake is considered a watershed event because of how damaged structures behaved during the tremors. In 1940, the United States was struck by an earthquake that measured 6.5 on the Richter scale and had the following f eatures.

Table (1) shows the results of the time history analysis of the frame under the El Centro earthquake of 1940 in OpenSees software.

Table 1. Validation results.

Ground Motion Imperial Valley-El Centro	Maximum Roof Displacement (mm) Welded Connections
Article Analysis	234
Verify Analysis	179

In Table (1), the maximum displacement of the roof was done in two modeling modes and obtained with appropriate approximation.

6. Sequence Earthquake Records in the Area far from the Fault

According to Table (2), three records were used to produce consecutive records.

As shown in Figures (8), (9) and (10), all the records have the same conditions regarding the type of soil and the area far from the fault.

Combined consecutive records with a time interval of 20 seconds are produced according to the individual records of Table (2) to apply sequence records to the structure according to Table (3) and Figures (11) to (13).

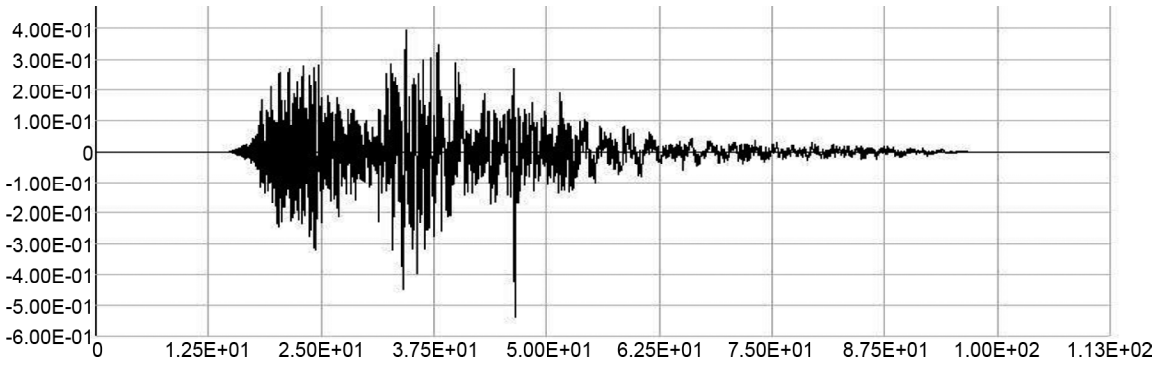

Figure 8. Acceleration map of El Mayor earthquake with a maximum ground acceleration equal to 538.0.

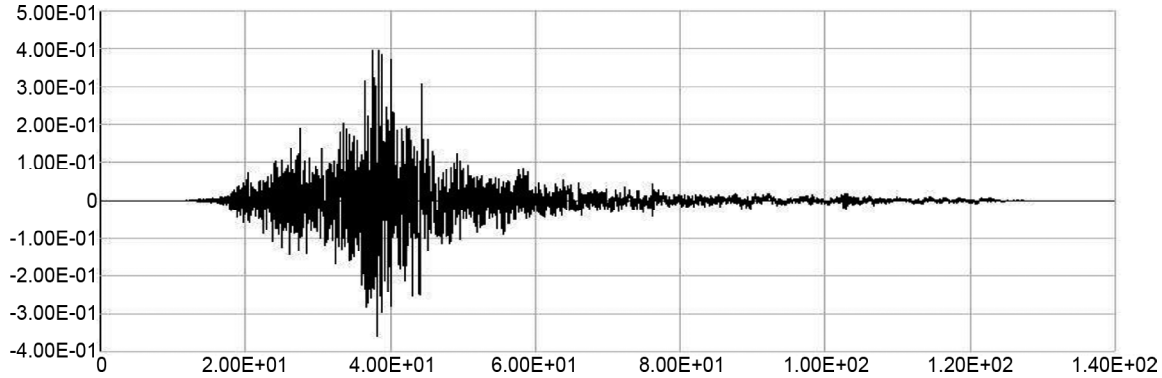

Figure 9. Acceleration map of El Mayor earthquake with a maximum ground acceleration equal to 0.390.

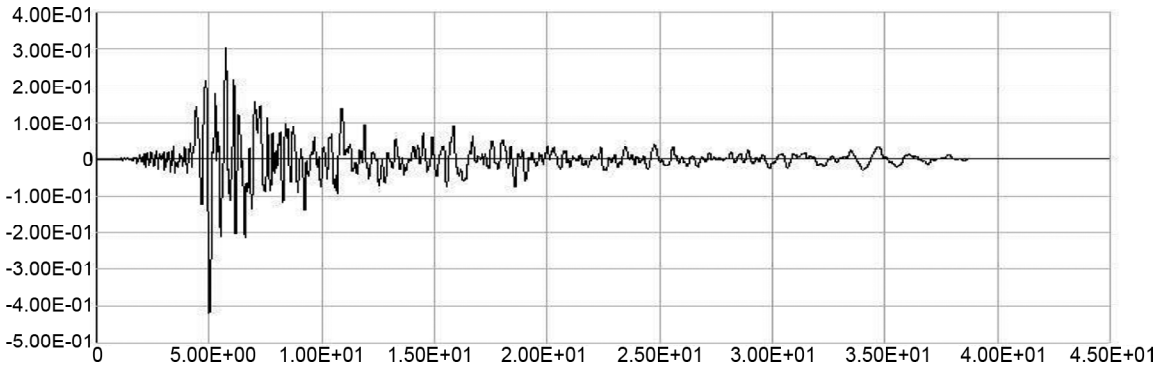

Figure 10. Acceleration map of Loma Prieta earthquake with maximum ground acceleration equal to 0.419.

Table 2. Specifications of records.

ID No.	Earthquake			Station Name	NEHRP Class	PGA Max (g)	d (km)
	M	Name	Year				
R1	7.2	El Mayor- Cucpah	2010	Riito	D	0.39	13.71
R2	7.2	El Mayor- Cucpah	2010	Michoacan De Ocampo	D	0.538	16.0
R3	6.9	Loma Prieta	1997	Gilro Array #4	D	0.419	14.34

Table 3. Combined records.

ID No.	Combined Details	Total Time (s)
Combinedrecordsery1	R2 + R1	249.99
Combinedrecordsery2	R2 + R3	159.985
Combinedrecordsery3	R1 + R3	189.985

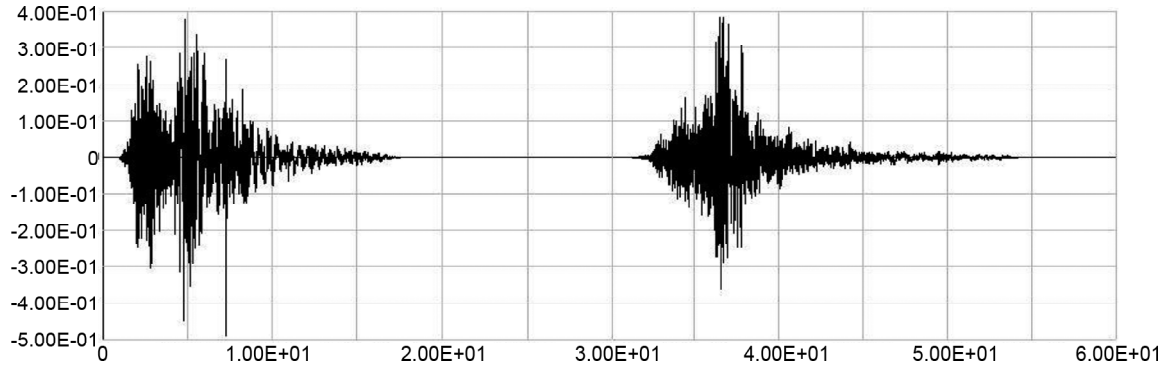

Figure 11. Acceleration mapping of the seismic sequence produced with the name Combinedrecordsery1.

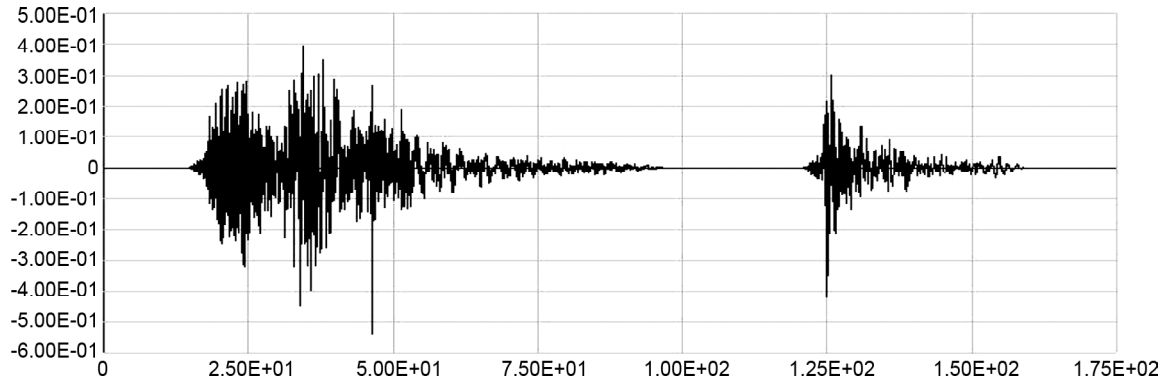

Figure 12. Acceleration mapping of the seismic sequence produced with the name Combinedrecordsery2.

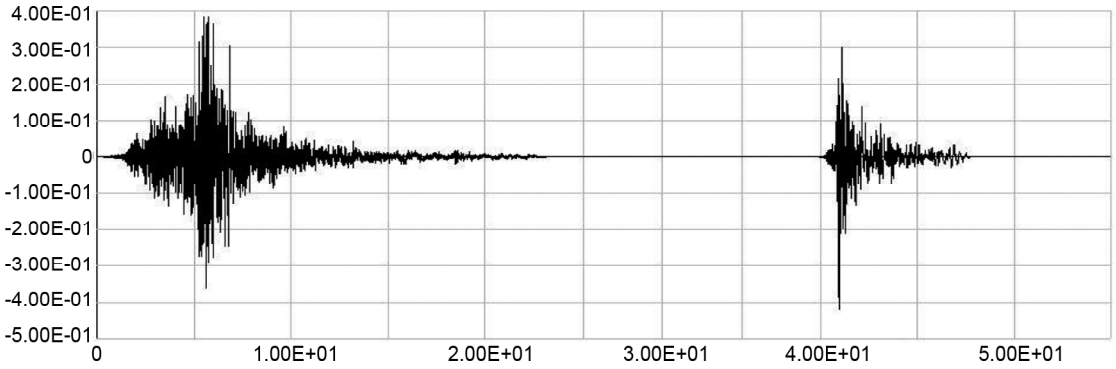

Figure 13. Acceleration mapping of the seismic sequence produced with the name Combinedrecordsery3.

7. Introduction of the Studied Structures

The system is evaluated using a steel flexural frame with pre-tensioned cables and two-dimensional steel flexural frames with three types of 5, 8, and 12 floors, respectively, for short, medium, and high order.

The selected models of 5, 8, and 12-story buildings that have the following specifications:

The soil of the type D or type III structure is considered according to the classification of the 2800 code of the fourth edition. The frames are considered two-dimensional and external frames. The structure in the X direction has three openings of 5 meters, and the height of the floors is 4.5 meters. The structure is in two modes: particular flexural frame and flexural frame with pretensioned cables, each classified into 5, 8, and 12 modes. The width of the loading frame is assumed to be 2.5 meters. The roof is believed to be a block beam type, and where the column is connected to the ground, it is supposed to be grounded. Beam and column members are considered A572 - Gr42. Young's modulus for Ecable cables should be 400000000 kg/cm^2. The Yang modulus for Edambar dampers is 80389018 kg/cm^2. Energy loss in dampers is regarded as 0.8. The yield stress value is f_y = 3000 kg/cm^2, the dead load is 540 kg/cm^2, and the live load is 200kg/cm^2. The designed dimensions and sections ar according to Figures (14) to (16) and Tables (4) to (6).

8. Results of Incremental Nonlinear Analysis

Incremental nonlinear analysis of three sequence records, Combinedrecordsery1, Combinedrecord-

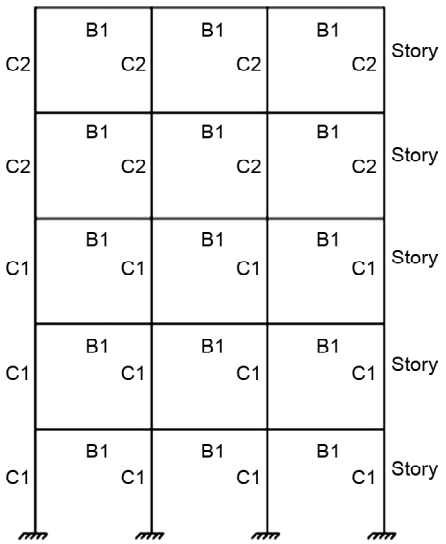

Figure 14. Beams and columns of the five-story frame.

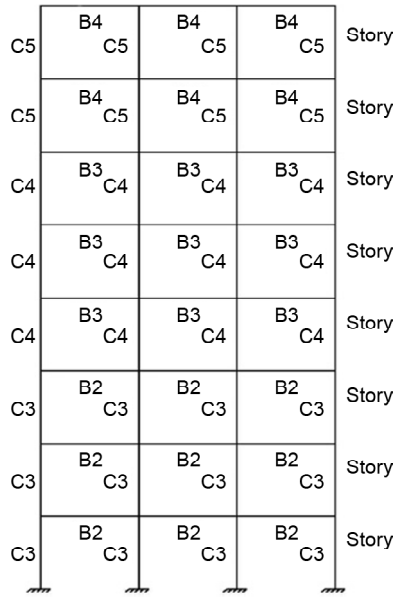

Figure 15. Beams and columns of the eight-story frame.

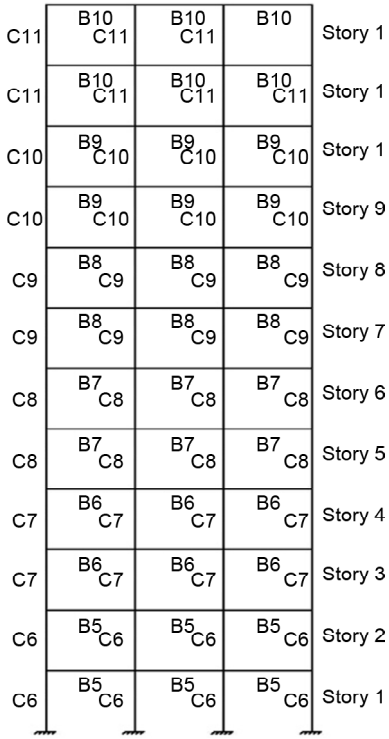

Figure 16. Beams and columns of the twelve-story frame.

Table 4. Introduction of flexural rigid frame structures.

Lable	Description	Range	
		Name	Stories
SM1L	Steal Moment Frame	Low-Rise	5
SM1M		Mid-Rise	8
SM1H		High-Rise	12

Table 5. Introduction of flexural rigid frame structures with pre-tensioned connections and cable connections.

Lable	Description	Range	
		Name	Stories
SM1L	Steal Moment Frame	Low-Rise	5
SM1M		Mid-Rise	8
SM1H		High-Rise	12

Table 6. Sections of beams and columns in ETABS software.

Columns		Beams	
Abbreviated Title	Section	Abbreviated Title	Section
W21×57	C1	W16×26	B1
W16×31	C2	W40×183	B2
W14×605	C3	W36×150	B3
W14×550	C4	W27×94	B4
W14×398	C5	W27×307	B5
W36×650	C6	W24×335	B6
W36×527	C7	W24×279	B7
W36×393	C8	W24×250	B8
W36×328	C9	W24×229	B9
W36×245	C10	W24×207	B10
W36×210	C11		

sery2, and Combinedrecordsery3, was performed with 5, 8, and 12-story frames with simple flexural joints and pre-tensioned connections.

8.1. Examining forms of Incremental Nonlinear Analysis

Figures (17) to (22) show the IDA diagrams and the average residual drift angle related to 5, 8 and 12-story frames with simple flexural joints (r_f) and flexural frames with pre-tensioned connections (p_t). At the beginning of the IDA graphs, there is an elastic area and a straight line, and part of the curve is the inter-section of all the curves. After this area, the non-linear behavior in the curves is shown by leaving the smooth line state.

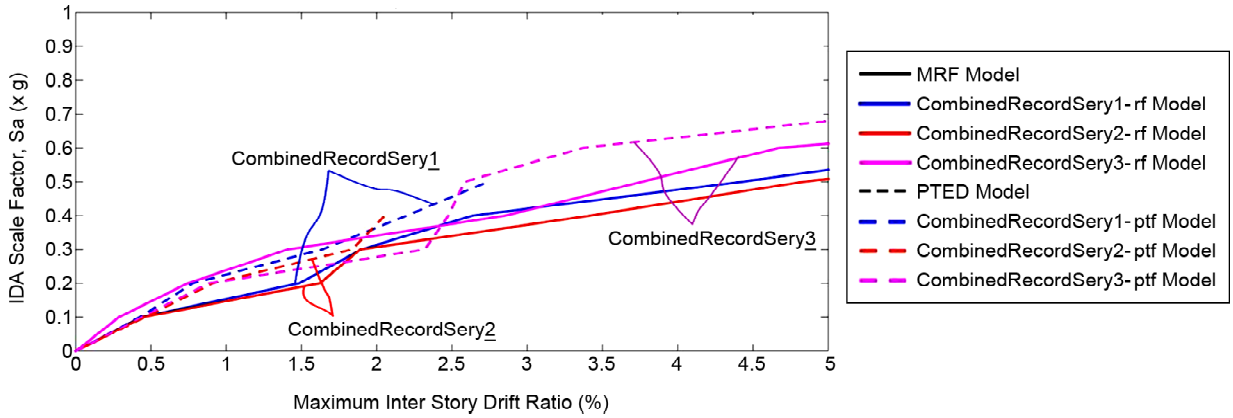

Figure 17. IDA curve of five-story structures.

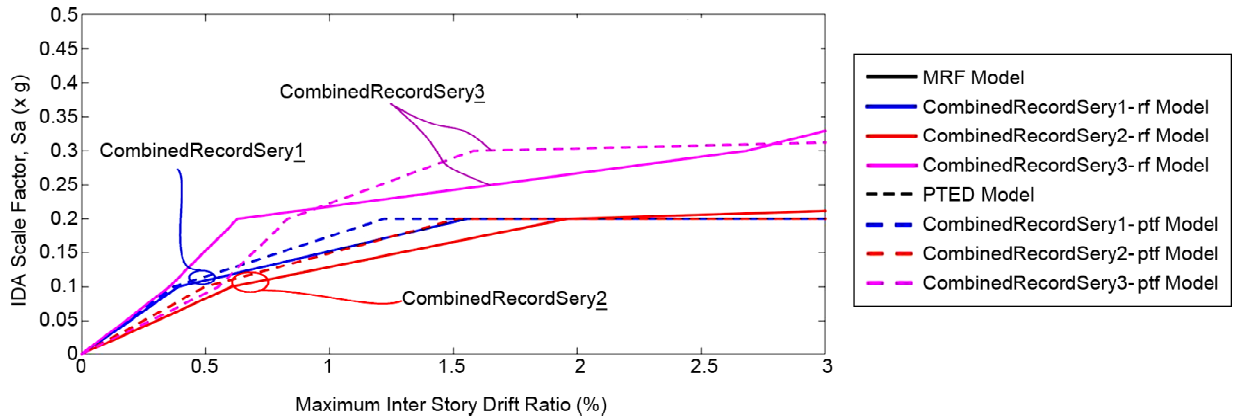

Figure 18. IDA curve of eight-story structures.

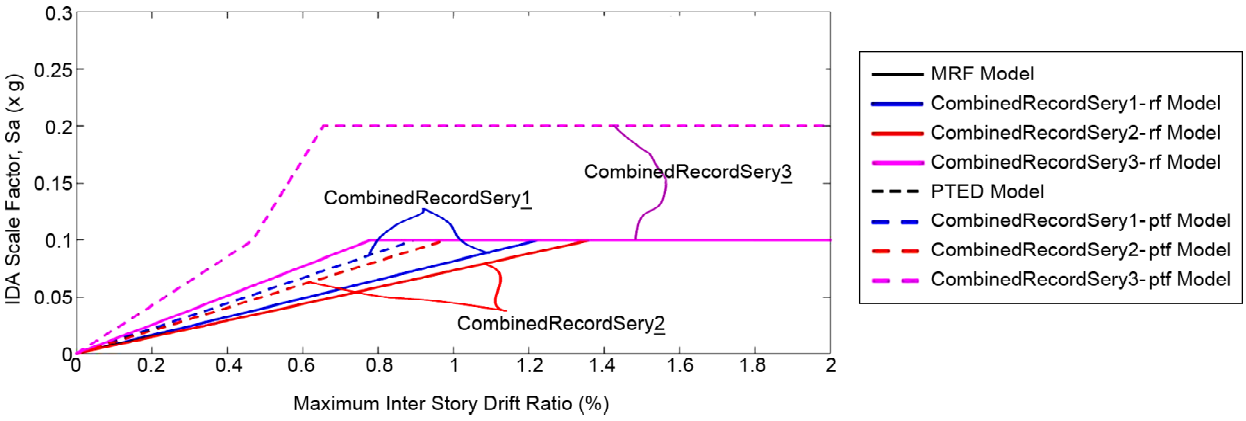

Figure 19. IDA curve of twelve-story structures.

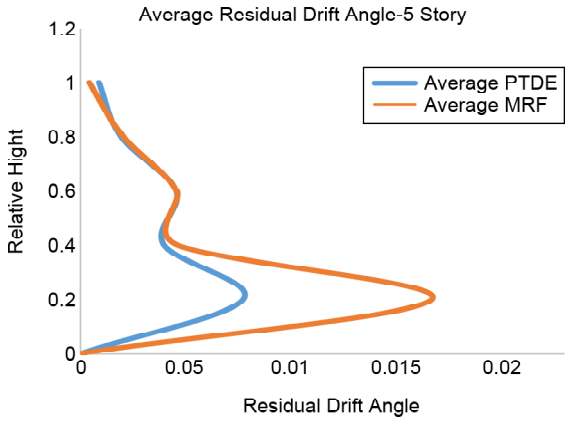

Figure 20. The diagram of the average relative displacement of floors in a five-story structure.

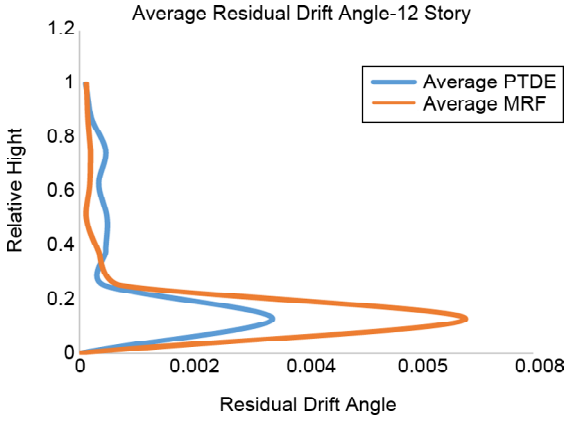

Figure 22. The diagram of the average relative displacement of floors in a twelve-story structure.

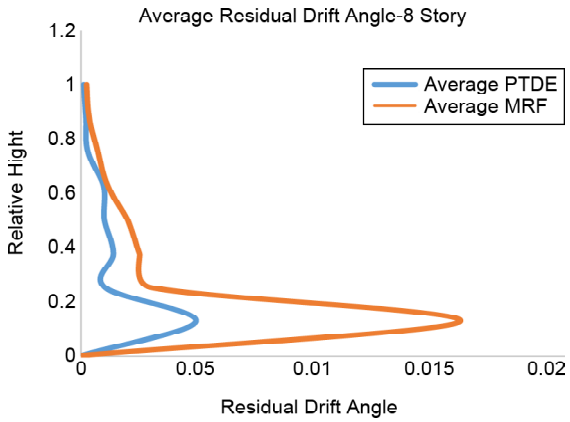

Figure 21. The diagram of the average relative displacement of floors in a eight-story structure.

According to the IDA shapes, shapes with post-tensioned connections are generally placed above the shapes with simple flexural connections. The amount of drifts is lower than that of simple flexural connections. In the frames of 5, 8, and 12 stories, they reach the overturning stage at the accelerations of 0.2g-0.4g, 0.4g-0.7g, and 0.28-0.1g, respectively, which indicates that the structure's performance decreases with the increase in height. On the other hand, in the shapes of the average maximum drift angle in the frames of 5, 8, and 12 floors on the first floor, the average values of the maximum receiving angle in the frames with pre-tensioned joints are 46%, 30%, and 49% respectively in the frames with simple flexural joints. In addition, the average shape of the residual drift angle in post-tensioned connections is less than that of simple flexural connections.

As the relative height increases, this difference decreases, which indicates the more appropriate performance of flexural frames with pre-tensioned connections compared to flexural frames with simple joints.

The maximum residual drift angle of 5, 8, and 12-story structures related to Figures (18), (20), and (22) is shown for further investigation in Figure (23). As can be seen, the maximum residual drift angle of the story structure is reduced. The

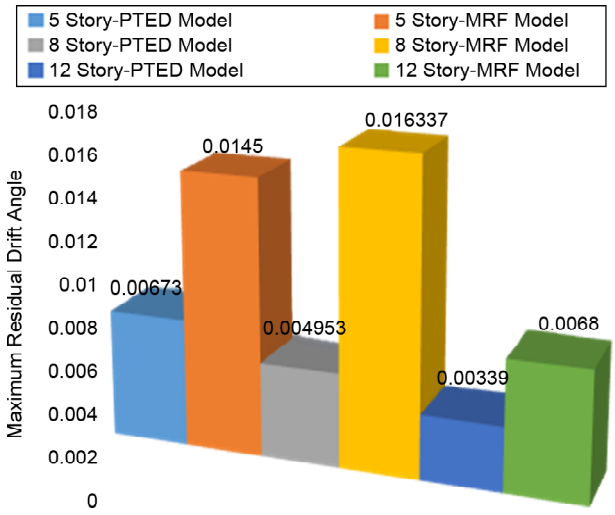

Figure 23. The maximum residual drift angle of 5, 8, and 12-story structures.

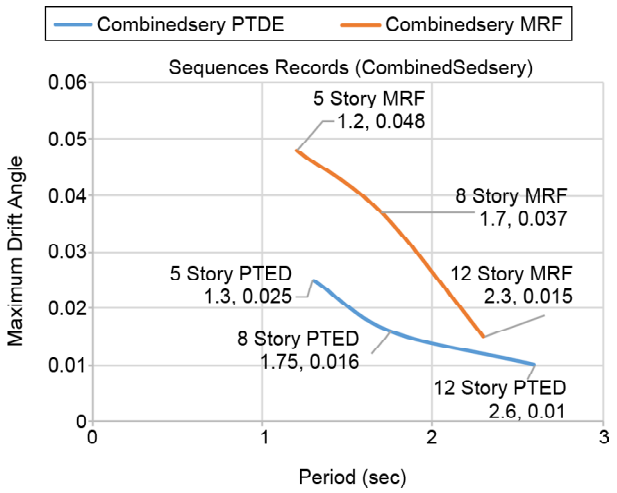

Figure 24. Rotation time - maximum relative displacement of floors in five-, eight-, and twelve-floor frames with pre-tensioned and simple flexural connections.

maximum residual drift angle of the 5-story MRF structure has been reduced from 0.0145 to 0.00673 in the PTED structure. In 8-story structures, a significant decrease from 0.004053 to 0.016377 can be observed similarly. On the other hand, comparing the extended structures of MRF and PTED, the maximum residual drift angle decreased from 0.0068 to 0.00330. Therefore, the proper performance of pre-tensioned connections is noticeable in tall structures, especially tall ones.

8.2. The form of Periodic Time at the Maximum Drift Angle

The cycle time-maximum drift angle figure (Figure 24) can be used to compare the performance of 5, 8 and 12-story frames in two cases: a rigid flexural frame with simple connections and a rigid flexural frame with pre-tensioned connections.

Figure (24) specifies the rotation time based on the maximum drift angle in the 5, 8 and 12-story frames in two cases of prestressed simple flexural rigid joints. Due to the longer cycle time in frames with pre-tensioned connections, the angle of maximum drifts is lower than the rigid frame with a simple flexural connection.

8.3. Investigating Incremental Nonlinear Analysis under Single Records

Figure (25) shows IDA diagrams for 5-, 8-, and 12-story fabs with simple, prestressed flexural

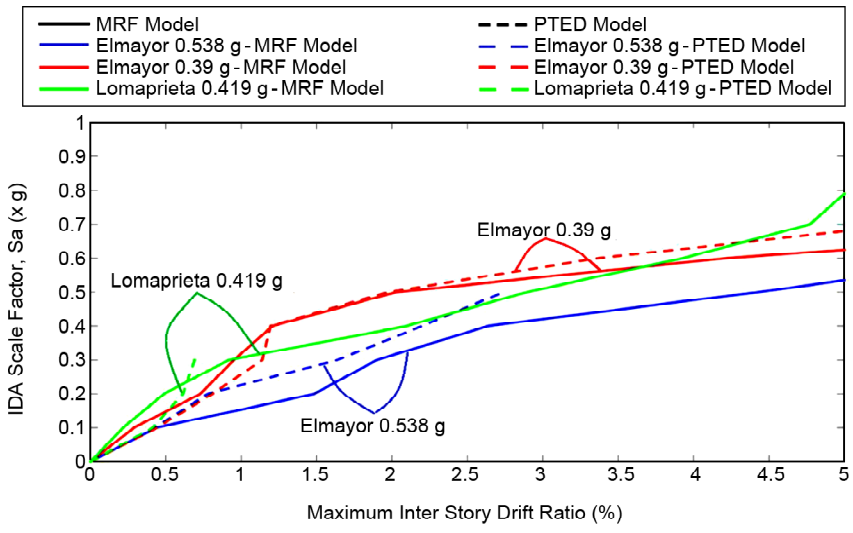

(a) 5-Story IDA

Figure 25. IDA charts under individual records.

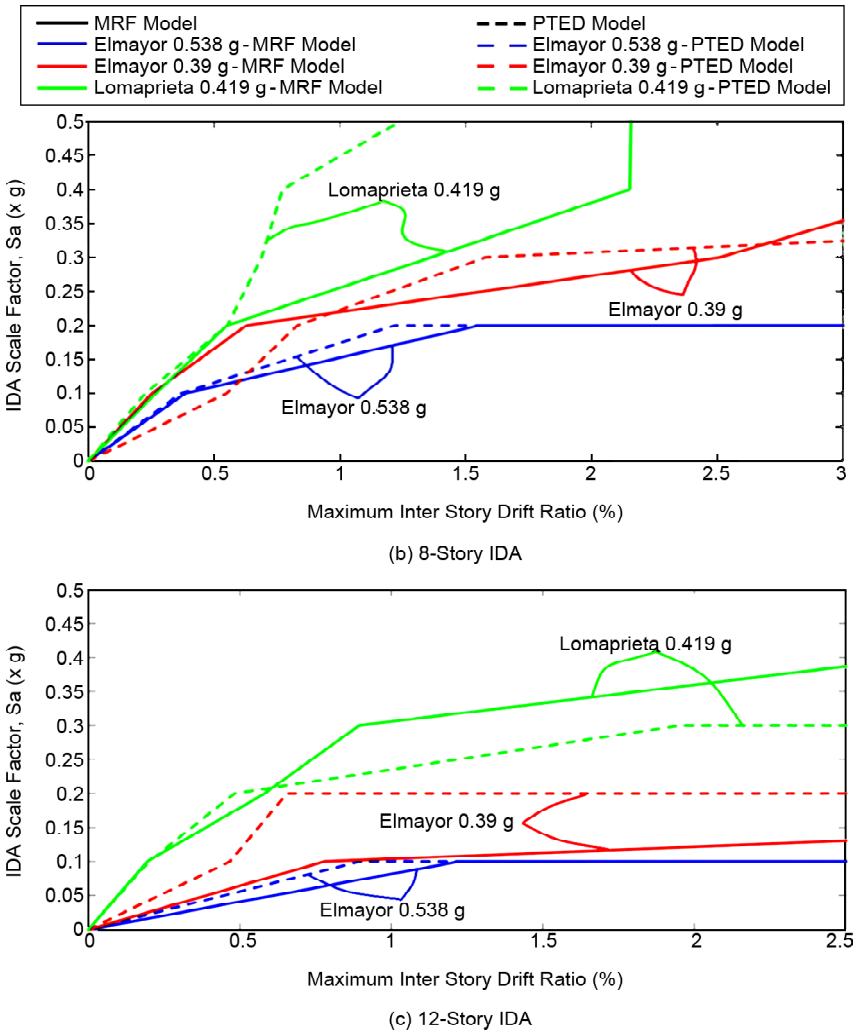

Figure 25. Continue.

joints under individual records. Initially, the graphs are in the elastic region, with a smooth line common to all graphs. After this area, non-linear behavior is observed. Graphs with simple flexural connections are lower than those with post-tensioned connections, and structures with prestressed flexural connections reach complete overturning at higher accelerations.

9. Conclusions

This study modeled 12-story structures with simple flexural joints and pre-tensioned connections to investigate the performance of tall structures with pre-tensioned connections under seismic sequences. For further investigation, 5- and 8-story structures were also modeled. On the other hand, the beam and column sections of the mentioned structures were calculated with ETABS software and simulated with OpenSees software for non-linear analysis. The studied structures were subjected to sequence earthquakes to perform nonlinear analysis, and the following results were obtained:

1. The diagrams of flexural joint tall structures are lower than those with IDA post-tensioned connections. Also, the graphs of the structures with flexural connections at lower levels under sequence and single records reach complete overturning compared to those with post-tensioned connections.
2. According to the results of sequence records, the maximum residual angle values in 5-, 8-, and 12-story structures have decreased by 53%, 69%, and 50%, respectively, with post-tensioned connections.
3. The maximum values of the relative lateral displacement of the floors compared to the frame are lower due to the longer rotation time of the frame with the pulled-back connections.
4. Bending with simple connections has been

considered, which indicates the more suitable performance of the stretched pad connections in the metal bending frame can limit the sequence of tremors in the area away from the fault.

5. Data from individual records shows that maximum drift angle values in 5-, 8-, and 12-story buildings have reduced by 48%, 57%, and 33%, respectively, when post-tensioned connections are used.
6. According to the IDE diagram in the individual records, the sarees with prestressed Nibet connections to simple bending connections withstand higher accelerations, leading to complete failure later.

Article Highlights

- Adding post-tensioned connections declines the maximum drift angle in tall buildings under sequence records.
- The post-tensioned connections significantly decrease the maximum residual angle in tall buildings.
- According to the IDA curve, the post-tensioned connections improve seismic performance in tall buildings under sequence records.

References

Akhavan Salmassi, M., Gerami, M., & Heidari Tafreshi, A. (2019). Evaluation of flexible steel frame structures with post-tensioned cables to sequences far from fault. *J. Struct. Constr. Eng.*, *6*(3), 221-234.

Al Kajbaf, A., Fanaie, N., & Najarkolaie, K.F. (2018). Numerical simulation of failure in steel post-tensioned connections under cyclic loading. *Eng. Fail. Anal., 91*, 35-57.

Apostolakis, G., Dargush, G.F., & Filiatrault, A. (2014). A computational framework for automated seismic design of steel frames with self-centering connections. *J. Comput. Civ. Eng.*, *28*(2), 170-181.

Azizi, M., & Siahpolo, N. (2019). Evaluating the effect of strength and geometry parameters of angle on behavior of post-tensioned steel connection with top and bottom angles. *J. Struct. Constr. Eng.*, *6*(2), 191-208.

Chancellor, N.B., Eatherton, M.R., Roke, D.A., & Akbas, T. (2014). The self-centering seismic lateral force resisting systems: high-performance structures for the city of tomorrow. *J. Build.*, *4*(3), 520-548.

Cheok, G.S., & Lew, H. (1991). Performance of precast concrete beam-to-column connections to cyclic loading. *PCI J.*, *36*(3), 56-67.

Chou, C.C., Chen, J.H., Chen, Y.C., & Tsai, K.C. (2006). Evaluating the performance of post-tensioned steel connections with strands and reduced flange plates. *Earthq. Eng. Struct. Dyn.*, *35*(9), 1167-1185.

Christopoulos, C., Filiatrault, A., & Folz, B. (2002). Seismic response of self-centering hysteretic SDOF systems. *Earthq. Eng. Struct. Dyn.*, *31*(5), 1131-1150.

Doostdar, H., Nemati, M., & Naghi Pour, M. (2010). Experimental study and modeling of reinforced concrete beams strengthened by post-tensioned external reinforcing bars. *Int. J. Eng.*, *23*(2), 127-144.

Fragiacomo, M., Amadio, C., & Macorini, L. (2004). Seismic response of steel frames under repeated earthquake ground motions. *Eng. Struct.*, *26*(13), 2021-2035.

Gerami, M., & Khatami, M. (2017). The effects of initial post tensioning force on seismic behavior of steel moment resisting frames by post-tensioned connections. *SJCE*, *33*(1.1), 107-115.

Guan, X., Burton, H., & Moradi, S. (2018). Seismic performance of a self-centering steel moment frame building: From component-level modeling to economic loss assessment. *J. Constr. Steel Res.*, *150*, 129-140.

Hatzigeorgiou, G.D. (2010). Ductility demand spectra for multiple near-and far-fault earthquakes. *Soil Dyn. Earthq. Eng.*, *30*(4), 170-183.

Kim, H.J., & Christopoulos C. (2008a). Numerical models and ductile ultimate deformation response of post-tensioned self-centering moment connections. *Earthq. Eng. Struct. Dyn.*, *38*(1), 1-21.

Kim, H.J., & Christopoulos, C. (2008b). Friction-damped post-tensioned self-centering steel moment-resisting frames. *J. Struct. Eng.*, *134*(11), 1768-1779.

Kurama, Y., Pessiki, S., Sause, R., & Lu, L.W. (1999). Seismic behavior and design of unbonded post-tensioned precast concrete walls. *PCI J.*, *44*(3), 72-89.

Lavaei, M.H., Dehcheshmeh, E.M., Safari, P., Broujerdian, V., & Gandomi, A.H. (2023). Reliability-based design optimization of post-tensioned self-centering rocking steel frame structures. *J. Build. Eng.*, 106955.

Lee, J., Lim, H., & Kim, C. (2020). Structural behavior of prestressed concrete beams with high-strength stirrups. *European Journal of Environmental and Civil Engineering*, *26*(5), 1722-1737.

Li, L.X., Li, C., & Hao, H. (2023). Seismic performance of post-tensioned self-centering concrete frames under near-fault pulse-like ground motions. *Eng. Struct.*, *277*, 115480.

Mazzoni, S., McKenna, F., Scott, M.H., Fenves, G.L., & Jeremic B. (2007). *Opensees Command Language Manual.*

Nateghi A.F., & Vatandoost, M. (2018). Seismic retrofitting RC structures with precast prestressed concrete braces-ABAQUS FEA modeling. *Int. J. Eng.*, *31*(3), 394-404.

Priestley, M.N., & Tao, J.R. (1993). Seismic response of precast prestressed concrete frames with partially debonded tendons. *PCI J.*, *38*(1), 58-69.

Ricles, J.M., Sause, R., Garlock, M.M., & Zhao, C. (2001). Posttensioned seismic-resistant connections for steel frames. *J. Struct. Eng.*, *127*(2), 113-121.

Ricles, J.M., Sause, R., Peng, S., Lu, L. (2002). Experimental evaluation of earthquake-resistant post-tensioned steel connections. *J. Struct. Eng.*, *128*(7), 850-859

Saberi, V., Gerami, M., & Kheyroddin, A. (2016). Seismic rehabilitation of bolted end plate connections using post-tensioned tendons. *Eng. Struct.*, *129*, 18-30.

Sarkisian, M.P. (2022). The impact of Jin Mao Tower on the life-cycle civil engineering of tall buildings. *Struct. Infrastruct. Eng.*, *18*(7), 895-932.

Sarvestani, H.A. (2017). Cyclic behavior of hexagonal castellated beams in steel moment-resisting frames with post-tensioned connections. *Struct. J.*

Shen, J., & Akbas, B. (1999). Seismic energy demand in steel moment frames. *J. Earthq. Eng.*, *3*(04), 519-559.

Tafreshi, A.M.H., & Gerami, M. (2021). Implementing post-tensioned connections only in some floors of steel moment frames. *Struct. J.*

Zhao, Z., Jian, X., Liang, B., & Liu, H. (2020). Progressive collapse assessment of friction-damped post-tensioned steel frames based on a simplified model. *Struct. J.*